Marine Geology
February 2020, Volume 420 Pages 106048 (13p.)
https://doi.org/10.1016/j.margeo.2019.106048
https://archimer.ifremer.fr/doc/00607/71925/

Decadal-scale morphological evolution of a muddy open coast

Orseau Sylvain [1, *], Zorrilla Noelia Abascal [2], Huybrechts Nicolas [1], Lesourd Sandric [3], Gardel Antoine [2]

[1] Cerema, Direct Tech Eau, 134 Rue Beauvais, Margny Les Compiegne, France.
[2] CNRS, LEEISA, USR 3456, 275 Route Montabo, F-97300 Cayenne, Guyane Francais, France.
[3] Univ Caen, M2C, UMR 6143, 24 Rue Tilleuls, F-14000 Caen, France.

Corresponding author : Sylvain Orseau, email address : sylvain.orseau@cerema.fr

noelia.abascal-zorrilla@cnrs.fr ; nicolas.huybrechts@cerema.fr ; sandric.lesourd@unicaen.fr ; antoine.gardel@cnrs.fr

Highlights

► Analysis of the long-term morphological evolution of a muddy open-coast ► Sediment transport suggests a growth of mudbanks migrating along the coast. ► Cross-shore exchange of sediment is equally significant as longshore transport. ► Mudbank and shoreline erosion/accretion trends are reversed.

1 Introduction

A muddy open coast is defined as a coastal sedimentary environment mainly composed of fine sediments (< 63µm in diameter) and formed along an unsheltered shoreline exposed to low energy conditions (Wang et al., 2002). These coastal environments are usually associated with rivers characterized by large sediment discharges such as the Amazon River, the Mississippi River, and several Asian rivers including the Yangtze, Ganges-Brahmaputra, Mekong, and Ayeyarwady Rivers. This continuous and abundant fine sediment supply is a prerequisite for the formation of an open muddy coast (Wang et al., 2002), while tide-wave interactions modulate the shape and extent of intertidal areas (Fan, 2012). These coastal environments share several similarities including extreme wave attenuation and rapid displacement of fluid mud (Wells, 1983).

Muddy open coasts are characterized by common morphological features depending on their dimensions and associated hydrodynamic forcing. In the seaward direction, the typical sequence of environments observed on an accreting muddy coast is: (i) swamps or chenier (beach) ridges, (ii) intertidal mudflats and (iii) shallow offshore muddy deposits. In tropical environments, swamps are mainly composed of mangrove forests that stabilize the intertidal area by enhancing sedimentation (Furukawa et al., 1997). Rarely, the upper intertidal area can be occupied by chenier ridges composed of sand and/or shelly material (Augustinus et al., 1989; Prost, 1989; Anthony et al., 2019).

The dynamics of a muddy open coast depend on the geographical area and are mainly driven by hydrological conditions. Along the southwest Indian coast of Kerala, during the rough monsoon season, high waves induce large resuspension and onshore fluid-mud advection, creating ephemeral mud banks (Kurup, 1977). The longest muddy open coast in the world is that of the Guianas, located in northeastern South America (Fig. 1), under the influence of the large sediment discharge from the Amazon (Anthony et al., 2010). Fine sediments are transported, in a unique system at the world scale, as large mud banks that migrate alongshore from the mouths of the Amazon in Brazil, towards those of

the Orinoco in Venezuela, mainly driven by trade-wind waves (NEDECO, 1968; Augustinus, 1978, 2004; Wells and Coleman, 1981a; Froidefond et al., 1988; Eisma et al., 1991; Allison et al., 2000; Gratiot et al., 2007). The mud transport processes and the interactions between mud banks and shoreline evolution constitute important challenges in terms of knowledge and data gaps on this unique muddy open coast of South America. As in many other muddy coasts of the world, issues related to coastal management are common on the Guianas coast, and are probably exacerbated by the pronounced impacts of mud concentration into distinct large migrating mud banks separated by so-called 'inter-bank' areas devoid of mud banks. These issues are becoming more and more prominent with climate change and carbon storage and release, as they involve large-scale mangrove removal or conservation (e.g., Brunier et al., 2019), and flood defenses (Anthony and Gratiot, 2012; Winterwerp et al., 2013), but also the maintenance of navigation channels that incur significant and costly dredging operations for harbours.

This paper addresses issues related to the morphology and dynamics of mud banks and their impact on shoreline change at a decadal scale of analysis. The Kaw Mud Bank was located along the French Guiana Coast between 2008 and 2018, and across the mouth of the small Mahury River, providing a unique opportunity and the proximity necessary for monitoring of bank dynamics. Sparse information exists on aspects of the mud bank subtidal area (NEDECO, 1968; Abascal Zorrilla et al., 2018), coupled with a better knowledge of changes in the shoreline and intertidal area (Anthony et al., 2010), but the interactions between mud banks, much of which are actually subtidal features, and decadal-scale shoreline change are much less well documented. Our study is aimed at contributing to a better understanding of this relationship which requires insight on: (1) mud-bank bathymetry and subtidal morphological changes, notably in the outer mud bank area, and (2) mud transport processes both alongshore, which corresponds to the classical model of mud-bank migration, and across-shore, necessary for shoreline change. We pay special attention to inter-annual changes in fluid-mud distribution and their interaction with the shoreline.

2 Settings

2.1 The mud-bank coast of South America

Mud banks migrating along the Guianas Coast are composed of sediments discharged by the Amazon River and are initially formed near Cabos Cassiporé and Orange, ~480km NW of the mouths of the Amazon (Allison et al., 2000, 1995; Gensac et al., 2016). This migration process involves several external forcings acting at different spatial and temporal scales (Fig. 2). The mouths and continental shelf of the Amazon are complex areas characterized by strong temporal and spatial variability (Nittrouer and DeMaster, 1996). This area was the focus of much of the early research on mud supply and advection along the Guianas coast, providing impetus for ground-breaking research on the processes of fluid-mud accumulation and fine-grained sedimentation. In this area, from 60 to 90% of suspended sediments can be in the form of dense nearbed fluid mud (Kineke et al., 1995; Kuehl et al., 1995) distributed over an area of ~10,000 km² depending on trade-wind wave intensity (Allison et al., 1995). About 15-20% of this fluid mud is reportedly advected along the Amapá-Guianas coast (Augustinus, 1978; Eisma et al., 1991; Wells and Coleman, 1977). The rest is deposited in the subaqueous delta of the Amazon (Kuehl et al., 1986), but also serves to build up mud banks that migrate toward the Orinoco Delta. These sediments are remobilized and transported alongshore by a complex combination of wave forcing, tidal currents, and wind-induced coastal currents (Allison et al., 2000; Augustinus, 2004; Eisma et al., 1991; Gratiot et al., 2007; NEDECO, 1968; Pujos et al., 1996; Wells et al., 1978, 1980; Wells and Coleman, 1977, 1981a). Fine sediments can be deposited along the Amapá-Guianas Coast with the aid of mangrove entrapment, resulting in the formation of mud capes (such as Pointe Behague in Fig. 1) and the progradation of tidal flats (Allison et al., 1995; Gensac et al., 2016; Nittrouer and DeMaster, 1996). However, this coastal sedimentation represents only a minor part of the total volume of sediment displaced by currents.

During their migration, mud banks exert a considerable influence on shoreline dynamics by creating conditions alternating between prograding and receding phases at sub-decadal to multi-decadal timescales (Allersma, 1971; Allison and Lee, 2004; Augustinus, 2004; Eisma et al., 1991; Froidefond et al., 1988; Plaziat and Augustinus, 2004), with the area around the mouth of the Sinnamary River (Fig. 1), 570-650 km northwest of the mouths of the Amazon, being the most active (Gratiot et al., 2008). During phases of retreat, shoreline erosion is homogeneous over long stretches of coast (Lefebvre et al., 2004), characterized by a jagged outline at the local scale (Anthony et al., 2010) with rates varying from 30-150 m/yr and exceptionally exceeding 200 m/yr (Gratiot et al., 2008; Brunier et al., 2019). During prograding phases, continuous supplies of fluid mud lead to the formation of mud bars that provide a substrate for pioneer mangroves, which enhance deposition and attenuate wave energy (Anthony et al., 2008; Gardel et al., 2011; Gensac et al., 2015). Near estuary mouths, several of which occur between the mouths of the two large rivers, an extensive mudflat can be formed at the updrift side (Lefebvre et al., 2004). The following hydro-meteorological factors have been identified to explain such temporal and spatial variability of the shoreline (Fig. 2): (i) trade-wind wave intensity and direction (Augustinus, 2004; Eisma et al., 1991; Gardel and Gratiot, 2005; Gratiot et al., 2007; Rodriguez and Mehta, 1998), (ii) solitary waves (Wells et al., 1978; Wells and Coleman, 1981a), (iii) the nodal tidal cycle (18.6yrs) (Gratiot et al., 2008; Wells and Coleman, 1981b), (iv) tidal and coastal currents (Bourret et al., 2008; Chevalier et al., 2008; Gibbs, 1976; Pujos and Froidefond, 1995), (v) the Northern Atlantic Oscillation (Walcker et al., 2015) and (vi) other secondary factors for which correlations have not been clearly demonstrated, e.g., sea-level variation (NEDECO, 1968; Wong et al., 2009) and irregular ENSO variation (Gratiot et al., 2008; Pujos et al., 1996).

Mud bank dimensions range from 10 to 30 km wide in the cross-shore direction and from 10 to 50 km long in the longshore direction (Augustinus, 1978; Augustinus et al., 1989; Eisma et al., 1991; Froidefond et al., 1988). Migration is restricted by coastal currents to a narrow band from the shoreline

to 10-30 km offshore. The mud banks migrate over a bed of relict consolidated mud (Pujos et al., 1996). On the inner shelf, currents are unidirectional at the surface, while bottom (< 15 m) currents are alternating under tidal influence (Eisma and van der Marel, 1971; Pujos and Froidefond, 1995). Alongshore, the outer part of a mud bank can be divided into two morphological areas: (i) a trailing edge where consolidated mud (bulk density ≥ 1350kg.m^{-3}) is eroded and liquefied, and (ii) a leading edge, where fluid mud (bulk density ≤ 1250kg.m^{-3}) from the trailing edge is advected by the longshore-current and where coastal erosion is prevented by wave damping (Winterwerp et al., 2007). In the inner mud bank and the intertidal areas, along a similar shore-parallel axis, the leading edge is characterized by extensive mudflats and wave-formed mud bars (Gardel et al., 2011), whereas the trailing edge is characterized by the erosion of consolidated relict mud bars, generating mud pebbles (Gensac et al., 2015), and also by the uprooting of mangrove trees along the shoreline.

The liquefaction of mud is induced by the cyclic action of waves and wave-induced bottom shear stress, which generates small elastic deformations and internal failures within the seabed, favouring the mobilization of mud (Anthony et al., 2010). Wave action tends to maintain the generated fluid mud and suspended sediments in shallow waters. In the leading edge, where fluid mud is deposited, a wave-dissipation rate of up to 96% has been reported on the Surinam Coast (Wells and Kemp, 1986).

2.2 Study area

The study area is located between 2-6°N and 52-57°W and covers the Mahury River (catchment size: 3615 km^2) estuary in French Guiana (Fig. 1). The Mahury estuary has a funnel-shaped morphology, and the adjacent updrift shoreline is characterized by temporal alternations of erosion and accretion, whereas the downdrift sector is stabilized by rocky outcrops that preclude downdrift (eastward) deflection of the mouth, frequently observed in many of the estuaries of the Guianas Coast (Jolivet et al., 2019). These rocks crop out as a series of islets off the coast. The climate is an equatorial

type alternating between rainy and dry seasons, respectively from December to July and from August to December. The rainfall in the study area varies between 2 and 3 $m.yr^{-1}$. The Guianas coast is in a low-pressure area characterized by the convergence of trade-winds towards the Intertropical Front. Winds are mainly active from December to May, with low to moderate speeds (mean annual average: $5m.s^{-1}$), and blow predominantly from the northeast. The Mahury has an annual fresh water discharge of $2.94x10^9$ m^3 for 2014 and seasonal values averaged around 31 $m^3.s^{-1}$ during the dry season and 170 $m^3.s^{-1}$ during the rainy season (Orseau et al., 2017). Waves are mainly generated by the seasonal trade winds, and significant wave heights > 1 m from December to April, while, the rest of the year is characterized by heights < 1 m. For 2015, the mean significant wave height and period were 0.96 m and 7.65 s, respectively. Occasional high waves generated by North Atlantic storms can attain the Guianas Coast and sometimes cause damage (van Ledden et al., 2009). Tides are semi-diurnal with a range varying from 0.90 to 2.50 m for neap to spring tides. Along the Guianas Coast, shore-normal tidal currents can locally attain 0.45 $m.s^{-1}$ (Bourret et al., 2008). In addition to the predominant role of waves in generating mud-bank migration on the Guianas coast, wind forcing, tidal currents, the North Brazil Current, and freshwater discharge from the numerous rivers also influence this migration process. Tidal currents can lead to balanced sediment fluxes along a cross-shore direction up to 5 km offshore. The North-Brazilian Current (NBC) is a geostrophic current that can transport mud particles northwestward discharged by the Amazon. Water discharge from the rivers can create a 'hydraulic-groyne' effect that induces rapid mud accumulation on the right side of the estuary during the passage of a mud bank (Anthony et al., 2013; Péron et al., 2013). Where water discharge is particularly high, as in the case of the Maroni River (Fig. 1; catchment size: 68,700 km^2; mean discharge: 1700 m^3/s), mud banks can be fully reworked in the course of their migration. This process results in mud deposits a few kilometers offshore of the mouth and reconstitution of the mud bank downdrift of the river mouth.

Sediments offshore of the mouth of the Mahury are fine-grained and characterized by clay minerals in proportions similar to those of the Amazon (Eisma and van der Marel, 1971; Pujos et al., 1996). The navigation channel of the lower Mahury estuary connects the unique commercial harbor of French Guiana to the open sea and is 15 km long and 120 m wide. To avoid siltation and to ensure a safe access to the harbor, the channel is dredged everyday using the Air and Water Injection Dredging (AIRSET) method. This hydrodynamic technique uses water jets and air to mobilize consolidated mud and to advect resuspended particles into the water column during ebb tides. The influence of dredging operations will be discussed in section 5.1. Sands are supplied by the river during the rainy season but the volume seems to be small.

Along the Guianas Coast, sediment transports are mainly driven by three type of currents: (i) the coastal drift generated by the wave refraction (ii) tidal currents balancing sediment fluxes along a cross-shore direction in a restricted area (up to 5 km offshore) and (iii) the North-Brazilian Current (NBC) delimiting the migration zone along the coast and transporting northwestward suspended sediments discharged by the Amazon.

3 Methods

3.1 Data acquisition

In situ measurements were conducted between 2008 and 2018, mainly in nearshore areas (for a water depth < 20 m) and in the estuary mouth, in order to document the morphological evolution of the outer mud bank and transport pathways of fine-grained sediments. These measurements included:

- Annual bathymetric surveys carried out by the Lighthouses and Beacons Service of French Guiana with a Knudsen 320 Ms echosounder over an area of 310 km^2 in coastal waters (Fig. 3a). The echo-sounder is a bi-frequency (24-210 kHz) single beam model dedicated to shallow water surveys and with a resolution of 1 cm for depths of 0-100 m. Due to an unstable signal response at the lowest

frequency, the echo-sounder was set at a frequency of 210 kHz corresponding to the water/fluid-mud interface. When measurements are acquired during calm conditions, raw data (not shown) do not display a significant difference between the frequencies, except for the navigation channel where a significant fluid-mud layer is frequently observed. In this case, the nautical depth was determined by lead-line soundings for a corresponding density of 1.27.

- Wet bulk density measurements acquired over the area covered by the bathymetric survey (**Fig. 3b**) during periods representative of high and low waves, respectively in February and December 2014, in order to characterize the distribution and the thickness of fluid-mud deposits. Shipboard surveys were conducted along > 100 vertical profiles with a DensiTune probe developed by Stema systems and based on the tuning fork principle. The technology determines the mud density by analyzing the tine vibration inside the mud. The probe is composed of piezoelectric elements applying and receiving signals at different frequencies. This phase shift between signals is induced by the tine vibration and the physical properties of the mud. The DensiTune probe used in this study has a resolution of 1 $g.l^{-1}$, a saturation level of 1500 $g.l^{-1}$, and was calibrated with local mud to provide accurate measurements (Groposo et al., 2015).

- Hydrological surveys comprising (i) water-level measurements collected every 10 minutes at tide-gauge stations, and (ii) wave measurements from buoys and collected sparsely at different locations from 8 to 22 km offshore between 2007 and 2016 (the furthest location is represented in Fig. 1). Wave characteristics from the WAVEWATCH III global model (Tolman, 2009) were extracted at 4.9°N and 307.8°E to address data gaps. Both tide and wave measurements were monitored and delivered by the Lighthouses and Beacons Service of French Guiana.

Satellite data was also used to monitor shoreline evolution and downloaded from the Earth Explorer data base (https://earthexplorer.usgs.gov/) for a scene covering the study area between 2008 and 2018. The images used in this study were collected by Landsat 5, 7 and 8 and have a spatial

191 resolution of 30 m. Shoreline is extracted from images by applying a soil-adjusted vegetation index
192 (Huete, 1988) to better delineate the water/mangrove limit. The computation of the index includes
193 reflectance of the red and near infrared bands and a soil brightness correction factor.

194 **3.2 Data processing**

195 The data collected during bathymetric surveys and the wet-bulk-density measurements were
196 post-processed with QGIS software to perform interpolations and volume computations. Interpolations
197 were performed with the Inverse Distance Weighting (IDW) deterministic method, which is well suited
198 for sparse and irregular point measurements. For bathymetric surveys, Digital Elevation Model (DEM)
199 subtractions were performed to determine yearly bed evolution since 2008 from the bathymetric data.
200 The subtraction results were then used to estimate volumes of displaced sediments in deposition and
201 erosion areas. In this analysis, elevation changes within ±0.5m as considered as potential errors in bed
202 detection and thus excluded from the computations.

203 For density surveys, bed surface density was determined by computing the averaged density
204 between 1100 and 1250 $kg.m^{-3}$ whenever the thickness of fluid mud was significant (> 20 cm), or by
205 finding the maximum density value if there was no fluid mud. The thicknesses of fluid-mud layers
206 were then computed for mud densities ranging from 1100 to 1250 $kg.m^{-3}$ (NEDECO, 1968). Due to the
207 cyclic action of waves, which generates pore-pressure build up (Trowbridge and Kineke, 1994), fluid-
208 mud thicknesses below 20 cm were excluded.

209 **4 Results**

210 **4.1 Mud-bank morphological evolution**

211 The bed morphology extracted from the 2016 bathymetric survey along the two cross-shore
212 transects (A-B in Fig. 1) showed a convex profile in the mud-bank zone characterized by an extensive
213 intertidal area up to 7 km offshore and a steep profile (from 0.15 to 0.28°) beyond 9 km (Fig. 4a). The
214 interbank zone was characterized by a linear profile (from 0.005 to 0.01°) interrupted by steps at 0.9

215 and 2.3 km from the shoreline, and by high intertidal areas inherited from the preceding mud bank. A
216 comparison of the interbank and bank profiles shows a similar step-like feature at the end of the
217 profiles, denoting an offshore extension limit at ~13 km. However, both subtidal profiles showed
218 reversed variations of water depth. For water depths > 5 m, the highest depth values were observed on
219 the bank profile, while for water depths < 5 m, the interbank profile was deeper. This difference
220 highlights the role of waves in planing down the cross-shore profile during the interbank phase.

221 The two transects emplaced to record the bed morphology of the inner and the outer mud bank
222 (Fig. 1) show that the former is characterized by depth values in the range ~+0.5 m due to massive
223 accretion at the leading edge (western part of the mud bank), whereas an irregular profile highlighting
224 intense erosion prevailed in the trailing edge (Fig. 4b). The navigation channel is also well captured at
225 7.5 km, characterized by a narrow path and a steep left side due to dredging operations during the
226 crossing of the mud bank. The latter profile shows the offshore mud bank extension at 9.5 km from the
227 shoreline. Rine and Ginsburg (1985) identified on a mud bank in neighbouring Suriname alternations
228 of massive structureless mud beds up to as much as 2 m thick, often exhibiting parallel, wavy and
229 lenticular laminations and, rarely, micro cross-lamination. Our profile shows a “bed” morphology with
230 a relatively constant water depth (~5 m) in the trailing edge (eastern part of the mud bank) and a
231 significant depth reduction of 2 m over a distance of ~10 km in the leading edge (western part of the
232 mud bank).

233 The survey of the mudbank started in 2008 and finished in 2018 with an interval of 1 year.
234 However in order to analyze only significant bed evolution associated with the bank during its crossing
235 of the estuary mouth, 5 DEM subtractions were carried out at two-year intervals between 2008 and
236 2018 (Fig. 5). The bathymetric changes in 2008-2010 clearly showed the arrival of the mud bank
237 comprising a migration front with a relatively high elevation exceeding +4 m (Fig. 5a). The trailing
238 edge was partly discernible in the eastern part of the surveyed area with a maximum erosion rate of

239 0.98 m.yr^{-1}. Areas subject to erosion were also observed along the navigation channel in the estuary
240 mouth, probably due to dredging activities. During this phase of migration, it was expected that the
241 mud bank influenced suspended sediment concentrations through the rapid displacement of fluid-mud
242 patches or the formation of a turbid plume.

243 In 2010-2012, the leading edge increased its extension to cover an area of about 111 km^2 (Fig.
244 5b). Over this area, deposits are homogeneous and the average of the colored surface is around +1.71 m
245 high. Two active erosion zones were noticed: at the outer limit of the mud bank, and closer to the
246 shoreline. In contrast, the estuary mouth remained relatively stable with minor erosion areas. Over the
247 period 2012-2014, a large portion of the mud bank crossed the navigation channel, inducing rapid bed
248 evolution (> 2.5 m), particularly along the navigation channel and in the estuary mouth (Fig. 5c). The
249 right side of the navigation channel and the harbour basin recorded massive deposition (+4.6 m), while
250 the left side of the navigation channel was still in erosion. In coastal waters, deposition occurred mainly
251 in the lowermost reaches of of the channel, between the offshore bedrock islets and in front of the
252 beaches of Montjoly (Fig. 1) where two mud bars were formed (Fig. 5c). During 2014-2016,
253 sedimentation in the estuary mouth is still significant, exceeding 1.5 m along the navigation channel
254 and in the harbour basin (Fig. 5d). Mud bars formed during previous years disappeared and were
255 replaced by an extensive mudflat bounding sandy beaches and stretching from the lower intertidal zone
256 to a few kilometers offshore, a situation typical of major bank phases when sandy beaches become
257 entirely mud-bound and completely muted in terms of beach morphodynamics (Anthony et al., 2002;
258 Anthony and Dolique, 2004). In 2016-2018, the trailing edge was located in the navigation channel and
259 near the islets where strong erosion of the muddy bed, attaining a maximum of -1.8 m, was observed
260 (Fig. 5e). This high level of erosion, which represents the maximum value over the last decade,
261 suggesting strong wave activity during this period. The estuary mouth was relatively stable and

sheltered from wave activity by the outer mud bank. The data for this period also show the effect of dredging operations in removing mud accumulating within the harbour basin.

To summarize, bathymetric survey data acquired over a decade (2008-2018) showed significant long-term bed evolution in the outer mud bank with contrasting morphological features specific to the leading and trailing edges. Extreme bed-level changes were observed along the front of the bank, comprising shore-parallel mud bars within the leading edge and up to 11 km off the coast, between 4 and 5 m water depths for the trailing edge (Fig. 5f).

4.2 Seasonal distribution of fluid mud

As highlighted in section 2.1, the formation of fluid mud is one of the main processes enabling mud-bank migration under the action of trade-wind and solitary waves. However, it also constitutes a major issue for port authorities with siltation problems. In rare cases, a high wave-energy event can lead to the complete muddy infilling of the navigation channel in only a few hours (Fig. 6). Monitoring of the wet bulk density with the DensiTune probe enabled us to characterize the rheology of the muddy bed and to determine the thickness of fluid-mud layers. During energetic wave events, the leading/trailing edge interface was clearly identifiable from the wet bulk density values of the bed. The leading edge was characterized by liquefied mud (< 1250 kg.m^{-3}) with a homogeneous spatial distribution and the lowest bulk density values in the navigation channel and in the estuary mouth, which acted as sediment traps (Fig. 7a). The trailing edge was characterized by the exposure of an older consolidated bed of relict mud (> 1400 kg.m^{-3}), with erosion prevailing at depths of between 2 and 8 m. The shape of this trailing edge was perpendicular to the orientation of incoming waves. In the nearshore zone, large fluid-mud patches were also observed with thicknesses > 2 m (profile 63 on the Fig. 7b).

During calm periods, the spatial distribution of the surface density was more heterogeneous even though fluid and consolidated mud were still predominant in leading and trailing edges,

286 respectively (Fig. 8a). Fluid-mud layers were maintained in the navigation channel with thicknesses of
287 ~50% of the water column (Fig. 8b) even though conditions were less turbulent. This persistence of
288 fluid mud suggests the influence of other physical processes that will be discussed in the next section.
289 Most of the relict mud (> 1400 $kg.m^{-3}$) was located in the most active erosion area between 4 and 5 m
290 water depth in the trailing edge. Compared to the high-energy period, the surface density in the inner
291 mud bank increased with values ranging from 1250 to 1400 $kg.m^{-3}$. The decrease in wave heights
292 reduced turbulence and allowed for the deposition of fine particles, which rapidly led to self-weight
293 consolidation. This is confirmed by the absence of significant fluid-mud layers except inside the
294 navigation channel (Fig. 8b**)**.

295 The computation of the fluid-mud thickness (density comprised between 1100 and 1250 $kg.m^{-3}$)
296 for calm periods indeed revealed that fluid-mud layers with a thickness < 20 cm occurred over 83% of
297 the area covered by our measurements (Fig. 9b). During energetic conditions (Fig. 9a) a thick fluid-
298 mud layer was also observed in the navigation channel with highest values (> 1.5 m) at the entrance of
299 the estuary mouth and in front of the beaches of Montjoly. Another important fluid-mud layer was
300 noticed near the shoreline in the trailing edge (Fig. 9a).

301 **5 Discussion**

302 **5.1 Inter-annual variability of the sediment balance**

303 As illustrated in Fig. 2, the migration of mud banks is driven by several sources of forcing
304 acting at different spatial and temporal scales. Among these forcings, wind-generated waves play a
305 predominant role in longshore transport by liquefying the muddy bottom and by maintaining cohesive
306 sediment in gel-like form (Allison et al., 2000; Augustinus, 2004; Eisma et al., 1991; Gratiot et al.,
307 2007; NEDECO, 1968; Rodriguez and Mehta, 1998, Wells et al., 1978; Wells and Coleman, 1981a,
308 1981b). Variability in the rate of migration is influenced by shoreline orientation (Augustinus, 1978;
309 Gardel and Gratiot, 2005), the effects of river flow on mud banks (Anthony et al., 2013; Jolivet et al.,

2019), and local shoreline irregularities (Gratiot et al., 2007). A clear seasonal component also influences the sediment balance. As noted from the distribution of fluid-mud over the outer mud bank, self-weight consolidation occurs seasonally when wave energy is weak. From January to April, frequent high waves lead to mud liquefaction and the transport “en masse” of fluid mud nearshore and in the leading edge. From May to December, long periods of low wave energy allow self-weight consolidation, favouring rapid shoreline advance.

To describe the influence of wind-generated waves on the sediment balance, deposited and eroded volumes computed from DEM differences in the maritime part and the estuary mouth are compared with a wave parameter describing the overall impact of waves (Fig. 10). Gratiot et al. (2007) extracted a wave ratio based on wave heights (H_0) and wave periods (T) following an earlier formulation by Rodriguez and Mehta (1998). Due to the partial coverage of the outer mud bank during 2008, 2010 and 2018 bathymetric surveys, the computation of yearly eroded and deposited volumes was performed between 2011 and 2017.

Mud mobilization shows a strong time-dependence with wave forcing (Fig. 10a) confirming earlier observations linking trade-wind waves and mud-bank migration (Augustinus, 2004; Gardel and Gratiot, 2005). In the maritime part, corresponding to the outer mud bank, masses of deposited and eroded sediment varied between 18 and 71.10^6 tons.yr^{-1} and between 1 and 63.10^6 tons.yr^{-1}, respectively. An exception concerned the period 2016-2017, characterized by high erosion while the wave forcing parameter was at its lowest. This intense erosion could be explained by the prolonged calm period preceding the onset of high waves in 2017 year, a condition that favours the remobilization of mud in large quantities (Gratiot et al., 2007). Another explanation may be the effect, on mud-bank migration, of the bedrock promontory of Cayenne (Fig. 1), the largest of the few rocky outcrops on the 1500 km-long Guianas coast. The Cayenne promontory comprises headland-bound fringing sandy beaches, where, as mentioned earlier, beach-welding of mud and eventual mangrove colonization of

such welded mud can occur during the passage of extremely large mud banks (Anthony et al., 2002; Anthony and Dolique, 2004), but is rare during normal bank activity (Anthony et al., 2010). The projecting rocky shoreline of Cayenne forces an offshore diversion of the mud-bank migration pathway (Anthony and Dolique, 2004), confirmed by our observations, and this probably contributes to keeping much of the mud in a fluid-like or in a semi-consolidated form favourable to rapid remobilization even under moderately energetic waves (Gratiot et al., 2007).

For the remaining five periods (1 to 5 in Fig. 10), there is a moderate degree of correlation with volumes deposited (r^2=0.64, N=5, $p < 0.001$). However, a lack of correlation is observed for eroded volumes (r^2= 0.07, N=5, $p < 0.001$). This can be explained by low eroded values when the wave-forcing parameter is highest (2014-2015: period n°4 in Fig. 10). This poor relationship between the wave-forcing parameter and the rate of mud-bank migration was also observed by Gratiot et al. (2007) who attributed it to miscellaneous factors such as the influence of local wave incidence on longshore sediment transport, and coastal irregularities (headlands, estuaries, etc.).The analysis of volumes deposited and eroded in the offshore area (as distinct from the estuary mouth) suggests a growth in mud-bank size over the study area with a volume of deposition several times larger (from 3 to 17 times) than that of erosion, attaining a maximum value of 142 x 10^6 m^3 (Fig. 11b). An exception concerns the period from 2016 to 2017 when the eroded volume was 15.3% larger than the deposited volume. This turnaround can be an artefact due to the partial bathymetric coverage of the outer mud bank, but could also be explained by the reasons given previously in the analysis of time dependence of mud mobilization with wave forcing. By computing mangrove shoreline changes adjacent to the rivers of French Guiana, Allison and Lee (2004) obtained an equilibrium between deposition and erosion over the study area, but also an increase in the volumes of sediment involved in migration, denoting mud-bank growth in the course of migration. Allison and Lee (2004) attributed this increase to external inputs of fine sediments derived from mud banks updrift or from interbank areas, but also noted that

358 mud-bank dimensions depended on the way coastline orientation affected wave incidence, in agreement
359 with Augustinus (1978). In another study, Gardel and Gratiot (2005) attributed this non-linearity to
360 complex interactions between coastline orientation and variations in wind orientation and intensity.

361 For the estuary mouth, the balance of deposited and eroded volumes is the opposite of that of
362 the offshore area with maximum deposition during 2012-2013 and 2015-2016. Thus, it is likely that the
363 siltation of the estuary mouth occurred before and after the passage of the mud bank under the
364 influence of wind-generated waves. However, volumes are ten times lower than those computed in the
365 maritime part with maximum values of 12.5×10^6 and 5.7×10^6 m^3 for deposited and eroded volumes,
366 respectively. To quantify volumes of sediment displaced during dredging operations with the AIRSET
367 method, a relation based on the total duration of such operations and a mean "efficiency" (6500 $m^3.h^{-1}$)
368 was defined. During migration across the estuary mouth, the total volumes of dredged sediment were
369 approximately 8.9 $\times 10^6$ and 10 $\times$ 10^6 m^3 for 2013 and 2014, respectively. These volumes are equivalent
370 to those computed from DEM differences for the estuary mouth (Fig. 10c), but are at least ten times
371 lower than those computed for the offshore area, indicating a moderate influence of such operations on
372 the sediment balance. Dredging operations do not affect the overall mud budget but induce
373 remobilization, and can, thus, influence the local sediment balance.

374 The estimated mass of sediments exchanged between the mud bank and the mangrove-
375 colonized shoreline is of the order of 6-26.10^6 $tons.yr^{-1}$ for each mud bank (Allison et al., 2004).
376 However, this only represents a minor part of the sediment volume displaced along the outer mud bank
377 during migration. When volumes computed in this study are converted into mass, considering a bulk
378 density of 1250 $kg.m^{-3}$ and a water content of 60% (NEDECO, 1968), the volume of deposition for one
379 bank is estimated at 18-71$\times 10^6$ $tons.yr^{-1}$, while the volume of erosion is estimated at 1-63.10^6 $tons.yr^{-1}$.
380 These results confirm the fact that the outer mud bank is the most active mud-bank area and the one
381 with the highest rate of sediment transport. Moreover, the maximum sediment exchange between the

shoreline and the mud bank is only twice less. Comparison with data from Allison et al. (2004) shows that cross-shore sediment exchanges between the shoreline and the mud bank are of the same order of magnitude as longshore exchanges. These findings suggest that cross-shore exchanges are significant enough to influence mud-bank migration more than has generally been assumed.

5.2 Interactions between mud bank and shoreline: New insights on mud-bank migration

Due to the need for considerable field experimental work and the constraints posed by the rapid migration of the outer mud bank, few field investigations have been conducted in this outer mud-bank area, although it is known to be the largest part of a typical mud bank (Abascal Zorrilla et al., 2018; NEDECO, 1968). Most of the earlier authors therefore considered a mud bank as a shore-welded feature wherein the shoreline dynamics are characterized by an advance-retreat pattern frequently associated with bank and interbank phases (Augustinus, 1978; Eisma et al., 1991; Froidefond et al., 1988; NEDECO, 1968). However, based on radiochemical inventories, Allison and Lee (2004) proposed a new model of migration wherein mud banks are disconnected from the shoreline and fluid-mud suspensions are advected shoreward during high-wave-energy events. This latter model was given preference by Anthony et al. (2010), and further confirmed by Anthony et al. (2014) and by Gratiot and Anthony (2016). In our configuration, the simultaneous analysis of the shoreline and of the dynamics of the 2 m-isobath (Fig. 11) demonstrates that mud-bank-shoreline interactions may be more important than assumed, which tends to confirm the model of migration proposed by Allison and Lee (2004).

The time evolution of the 2 m-isobath clearly shows the migration of the leading edge of the bank from the Kaw River to 22 km westward off the rocky promontory of Cayenne (Fig. 11a). In the latter area, the 2 m-isobath describes a net seaward progression of up to 6 km and with rates varying between 0.54 and 2.56 $km.yr^{-1}$ between 2010 and 2016, thus illustrating the influence of the seaward projection of the Cayenne headland on mud-bank migration. Since 2016, erosion has prevailed off the mouth of the Mahury River due to the migration of the mud bank between kilometers 18 and 25 (Fig.

406 11b), and this has called for an intensification of dredging operations since then. In the present trailing
407 edge, the retreat of the outer mud bank is more homogeneous. Since 2012, the 2 m-isobath is receding
408 at rates lower than those computed for the present leading edge, and comprised between 0.3 and 1.2
409 $km.yr^{-1}$.

410 At the same time, the shoreline shows a reverse dynamic with: (i) the presence of a mud cape
411 deflecting the mouth of the Kaw River (Lefebvre et al., 2004), and (ii) rapid shoreline advance and
412 mangrove colonization between the Kaw and Mahury Rivers since 2014 (Fig. 11c). Such rapid
413 shoreline advance is commonly characterized by massive mud deposition between offshore bars and
414 the shoreline, as shown by Anthony et al. (2008) and Gensac et al. (2015). Between the mouths of the
415 Kaw and the Mahury, the pattern of mangrove colonization describes an arc in plan shape characteristic
416 of the offshore delimitation by the mud bar (Fromard et al., 2004). The rapid ensuing mangrove
417 colonization of the intertidal area between the shoreline and the mud bar required a large volume of
418 fluid mud that could only be provided by erosion of the outer mud bank.

419 The analysis of the 2 m-isobath and of shoreline evolution denotes a reverse dynamic
420 confirming the significance of cross-shore exchanges between the outer mud bank and the shoreline
421 during the migration of mud banks, in agreement with Allison et al. (2004). In the first few kilometers
422 of the leading edge, shoreline erosion can contribute to deposition in both the inner and outer parts of
423 the mud bank, and this potentially leads to a difference between deposited and eroded volumes of
424 sediments. In the last kilometers of the trailing edge, the shoreline advances with the help of mangrove
425 colonization while erosion prevails in the outer mud bank. This observation also implies that the
426 rhythmic pattern of shoreline advance and retreat generally observed is not suitable for describing the
427 dynamics of subtidal areas and, therefore, bank-interbank phases.

428

6 Conclusions

The measurements collected along part of the Amazon-influenced coast of South America have enabled us to describe the mesoscale (decade) morphological evolution of a muddy open coast exposed to ocean waves. The results provide new insight into the sediment transport pathway between migrating mud banks and the shoreface, and, more particularly, into the dynamics of the the subtidal area of a mud bank. This study has succeeded in characterizing the dynamics of the outer mud bank, which is equated with the subtidal part of a mud bank. The analysis of data from bathymetric surveys has allowed us to divide the outer mud bank into two main areas identified by an extensive linear mudflat in the leading edge (western part of a mud bank) and a deepening and irregular bed in the trailing edge (eastern part of a mud bank). Bed changes over a 10-yr period describe a rapid migration characterized by a steep leading-edge front where deposition is at a maximum and a linear shore-parallel erosion area between 4 and 5 m water depth.

The sediment balance estimated from bathymetric differentials show a strong inter-annual variation related to wave forcing, and the outer part of the mud bank is its most active part. Sediment exchanges between the shoreline and the mud bank (cross-shore) are of the same order of magnitude as in the longshore dimension (migration of leading and trailing edges), and the differentials computed for sediment volumes of the leading and trailing edges suggest an increase in the size of the mud bank during its migration. This increase could be explained by external inputs of sediment from updrift mud banks and by erosion of interbank areas. Simultaneous analysis of the shoreline and the 2 m-isobath highlights reverse dynamics and significant interactions between the outer mud bank and the adjacent shoreline. This involves initial erosion of the shoreline in the leading edge, releasing mud that contributes to more deposition in both the inner and outer parts of the mud bank, and this potentially leads to a difference between deposited and eroded volumes of sediments. Conversely, in the trailing edge, the shoreline initially advances with the help of mangrove colonization while erosion prevails in the outer mud bank. This reverse dynamic between the outer mud bank and the shoreline tends to

confirm that mud banks are disconnected from the shoreline, as initially suggested by the model of mud-bank migration proposed by Allison and Lee (2004). The rate of shoreline advance is driven by several factors, but seems to be very sensitive to wave influence on the bed, as noted by Gratiot et al; (2007). The inter-annual variations in mud-bank sediment transport and budgets analyzed in this study will help to calibrate future morphodynamic models of muddy open coasts, notably with regards to the rapid and significant shoreline variations. They will also be useful in management considerations relating to such shoreline fluctuations and to harbour siltation and maintenance.

Acknowledgements

This work was supported by the National Center for Scientific Reasearch (CNRS) of French Guiana. The authors thank the Lighthouses and Beacons Service of French Guiana and the Environment, Planning and Housing agency of French Guiana for providing data from the bathymetric surveys and wave measurements. The authors also thank the company Baggerbedrijf *de Boer* – Dutch Dredging for accompanying us with the use of the DensiTune and for shipboard measurements. Three reviewers, among whom Charles Nittrouer, and Editor-in-Chief Shu Gao provided insightful comments on the manuscript.

References

Abascal Zorrilla, N., Vantrepotte, V., Gensac, E., Huybrechts, N., Gardel, A., 2018. The Advantages of Landsat 8-OLI-Derived Suspended Particulate Matter Maps for Monitoring the Subtidal Extension of Amazonian Coastal Mud Banks (French Guiana). Remote Sens. 10, 1733. https://doi.org/10.3390/rs10111733

Allersma, E., 1971. Mud on the oceanic shelf off Guiana. Presented at the Symp. Invest. Resour. Caribb. Sea and adjacent Reg., UNESCO, Paris, pp. 193–203.

Allison, M.A., Lee, M.T., 2004. Sediment exchange between Amazon mudbanks and shore-fringing mangroves in French Guiana. Mar. Geol., 208, 169–190. https://doi.org/10.1016/j.margeo.2004.04.026

Allison, M.A., Lee, M.T., Ogston, A.S., Aller, R.C., 2000. Origin of Amazon mudbanks along the northeastern coast of South America. Mar. Geol. 163, 241–256. https://doi.org/10.1016/S0025-3227(99)00120-6

Allison, M.A., Nittrouer, C.A., Faria, L.E.C., 1995. Rates and mechanisms of shoreface progradation and retreat downdrift of the Amazon river mouth. Mar. Geol., 125, 373–392. https://doi.org/10.1016/0025-3227(95)00020-Y

Anthony, E.J., Brunier, G., Gardel, A., Hiwat, M., 2019. Chenier morphodynamics on the Amazon-influenced coast of Suriname, South America: Implications for beach ecosystem services. Front. Earth Sci. 7, 35, https://doi.org/10.3389/feart.2019.00035

Anthony, E.J., Dolique, F., 2004. The influence of Amazon-derived mud banks on the morphology of sandy headland-bound beaches in Cayenne, French Guiana: a short- to long-term perspective. Mar. Geol., 208, 249–264. https://doi.org/10.1016/j.margeo.2004.04.011

Anthony, E.J., Dolique, F., Gardel, A., Gratiot, N., Proisy, C., Polidori, L., 2008. Nearshore intertidal topography and topographic-forcing mechanisms of an Amazon-derived mud bank in French Guiana. Cont. Shelf Res. 28, 813–822. https://doi.org/10.1016/j.csr.2008.01.003

Anthony, E.J., Gardel, A., Dolique, F., Guiral, D., 2002. Short-term changes in the plan shape of a sandy beach in response to sheltering by a nearshore mud bank, Cayenne, French Guiana. Earth Surf. Process. Landf., 27, 857-866. http://onlinelibrary.wiley.com/doi/10.1002/esp.357/full

Anthony, E.J., Gardel, A., Gratiot, N., 2014. Fluvial sediment supply, mud banks, cheniers and the morphodynamics of the coast of South America between the Amazon and Orinoco river mouths. Geological Society, London, Special Publications, 388, 533–560. https://doi.org/10.1144/SP388.8

Anthony, E.J., Gardel, A., Gratiot, N., Proisy, C., Allison, M.A., Dolique, F., Fromard, F., 2010. The Amazon-influenced muddy coast of South America: A review of mud-bank–shoreline interactions. Earth-Sci. Rev. 103, 99–121. https://doi.org/10.1016/j.earscirev.2010.09.008

Anthony, E.J., Gardel, A., Proisy, C., Fromard, F., Gensac, E., Peron, C., Walcker, R., Lesourd, S., 2013. The role of fluvial sediment supply and river-mouth hydrology in the dynamics of the muddy, Amazon-dominated Amapá–Guianas coast, South America: A three-point research agenda. J. South Am. Earth Sci., 44, 18–24. https://doi.org/10.1016/j.jsames.2012.06.005

Anthony, E.J., Gratiot, N., 2012. Coastal engineering and large-scale mangrove destruction in Guyana, South America: Averting an environmental catastrophe in the making. Ecol. Eng., 47, 268-273. https://doi.org/10.1016/j.ecoleng.2012.07.005

Augustinus, P.G.E.F., 2004. The influence of the trade winds on the coastal development of the Guianas

at various scale levels: a synthesis. Mar. Geol., 208, 145–151. https://doi.org/10.1016/j.margeo.2004.04.007

Augustinus, P.G.E.F., 1978. The changing shoreline of Surinam (South America). Utrecht.

Augustinus, P.G.E.F., Hazelhoff, L., Kroon, A., 1989. The chenier coast of Suriname: Modern and geological development. Mar. Geol., 90, 269–281. https://doi.org/10.1016/0025-3227(89)90129-1

Bourret, A., Devenon, J.-L., Chevalier, C., 2008. Tidal influence on the hydrodynamics of the French Guiana continental shelf. Cont. Shelf Res. 28, 951–961. https://doi.org/10.1016/j.csr.2008.01.008

Brunier, G., Anthony, E.J., Gratiot, N., Gardel, A., 2019. Exceptional rates and mechanisms of muddy shoreline retreat following mangrove removal. Earth Surf. Process. Landf., 44, 1559-1571. https://doi.org/10.1002/esp.4593

Chevalier, C., Froidefond, J.M., Devenon, J.L., 2008. Numerical analysis of the combined action of littoral current, tide and waves on the suspended mud transport and on turbid plumes around French Guiana mudbanks. Cont. Shelf Res. 28, 545–560. https://doi.org/10.1016/j.csr.2007.09.011

Eisma, D., Augustinus, P.G.E.F., Alexander, C., 1991. Recent and subrecent changes in the dispersal of amazon mud. Neth. J. Sea Res. 28, 181–192. https://doi.org/10.1016/0077-7579(91)90016-T

Eisma, D., van der Marel, H.W., 1971. Marine muds along the Guyana coast and their origin from the Amazon basin. Contrib. Mineral. Petrol. 31, 321–334. https://doi.org/10.1007/BF00371152

Fan, D., 2012. Open-Coast Tidal Flats, in: Davis, R.A., Dalrymple, R.W. (Eds.), Principles of Tidal Sedimentology. Springer Netherlands, Dordrecht, pp. 187–229. https://doi.org/10.1007/978-94-007-0123-6

Froidefond, J.M., Pujos, M., Andre, X., 1988. Migration of mud banks and changing coastline in French Guiana. Mar. Geol. 84, 19–30. https://doi.org/10.1016/0025-3227(88)90122-3

Fromard, F., Vega, C., Proisy, C., 2004. Half a century of dynamic coastal change affecting mangrove shorelines of French Guiana. A case study based on remote sensing data analyses and field surveys. Mar. Geol., 208, 265–280. https://doi.org/10.1016/j.margeo.2004.04.018

Furukawa, K., Wolanski, E., Mueller, H., 1997. Currents and sediment transport in mangrove forests. Estuar. Coast. Shelf Sci. 44, 301–310. https://doi.org/10.1006/ecss.1996.0120

Gardel, A., Gensac, E., Anthony, E.J., Lesourd, S., Loisel, H., Marin, D., 2011. Wave-formed mud bars: their morphodynamics and role in opportunistic mangrove colonization. J. Coast. Res., Special Issue 64, 384–387.

Gardel, A., Gratiot, N., 2005. A satellite image–based method for estimating rates of mud bank migration, French Guiana, South America. J. Coast. Res., 21, 720–728. https://doi.org/10.2112/03-0100.1

Gensac, E., Gardel, A., Lesourd, S., Brutier, L., 2015. Morphodynamic evolution of an intertidal mudflat under the influence of Amazon sediment supply – Kourou mud bank, French Guiana, South America. Estuar. Coast. Shelf Sci. 158, 53–62. https://doi.org/10.1016/j.ecss.2015.03.017

Gensac, E., Martinez, J.-M., Vantrepotte, V., Anthony, E.J., 2016. Seasonal and inter-annual dynamics of suspended sediment at the mouth of the Amazon river: The role of continental and oceanic forcing, and implications for coastal geomorphology and mud bank formation. Cont. Shelf Res. 118, 49–62. https://doi.org/10.1016/j.csr.2016.02.009

Geyer, W.R., Beardsley, R.C., Lentz, S.J., Candela, J., Limeburner, R., Johns, W.E., Castro, B.M., Dias Soares, I., 1996. Physical oceanography of the Amazon shelf. Cont. Shelf Res. 16, 575–616. https://doi.org/10.1016/0278-4343(95)00051-8

Gibbs, R.J., 1976. Amazon River sediment transport in the Atlantic Ocean. Geology 4, 45–48. https://doi.org/10.1130/0091-7613(1976)4<45:ARSTIT>2.0.CO;2

Gratiot, N., Anthony, E.J., 2016. Role of flocculation and settling processes in the geological development of the mangrove-colonized, Amazon-influenced mud-bank coast of South America. Mar. Geol., 373, 1-10. https://doi.org/10.1016/j.margeo.2015.12.013

Gratiot, N., Anthony, E.J., Gardel, A., Gaucherel, C., Proisy, C., Wells, J.T., 2008. Significant contribution of the 18.6 year tidal cycle to regional coastal changes. Nat. Geosci. 1, 169–172. https://doi.org/10.1038/ngeo127

Gratiot, N., Gardel, A., Anthony, E.J., 2007. Trade-wind waves and mud dynamics on the French Guiana coast, South America: Input from ERA-40 wave data and field investigations. Mar. Geol. 236, 15–26. https://doi.org/10.1016/j.margeo.2006.09.013

Groposo Valentina, Mosquera Rodrigo L., Pedocchi Francisco, Vinzón Susana B., Gallo Marcos, 2015. Mud Density Prospection Using a Tuning Fork. J. Waterw. Port Coast. Ocean Eng. 141, 04014047. https://doi.org/10.1061/(ASCE)WW.1943-5460.0000289

Huete, A., 1988. A soil-adjusted vegetation index (SAVI). Rem. Sens. of Env., 25(3), 295-309. https://doi.org/10.1016/0034-4257(88)90106-X

Jolivet, M., Anthony, E.J., Gardel, A., Brunier, G., 2019. Multi-decadal to short-term beach and shoreline mobility in a complex river-mouth environment affected by mud from the Amazon. Frontiers in Earth Science, 7, 187. https://doi.org/10.3389/feart.2019.00187

Kineke, G.C., Sternberg, R.W., Trowbridge, J.H., Geyer, W.R., 1996. Fluid-mud processes on the Amazon continental shelf. Cont. Shelf Res. 16, 667–696. https://doi.org/10.1016/0278-4343(95)00050-X

Kuehl, S.A., DeMaster, D.J., Nittrouer, C.A., 1986. Nature of sediment accumulation on the Amazon continental shelf. Cont. Shelf Res., 6, 209–225. https://doi.org/10.1016/0278-4343(86)90061-0

Kuehl, S.A., Nittrouer, C.A., Allison, M.A., Faria, L.E.C., Dukat, D.A., Jaeger, J.M., Pacioni, T.D., Figueiredo, A.G., Underkoffler, E.C. 1996. Sediment deposition, accumulation, and seabed dynamics in an energetic fine-grained coastal environment. Cont. Shelf Res., 16, 787–815. https://doi.org/10.1016/0278-4343(95)00047-X

Kurup, P.G., 1977. Studies on the physical aspects of the mud banks along the Kerala coast with special refrence to the Purakad mud bank (Bulletin). Dep. Mar. Sci. Univ. Cochin.

Lefebvre, J.P., Dolique, F., Gratiot, N., 2004. Geomorphic evolution of a coastal mudflat under oceanic influences: an example from the dynamic shoreline of French Guiana. Mar. Geol., 208, 191–205. https://doi.org/10.1016/j.margeo.2004.04.008

NEDECO, 1968. Surinam transportation study: Report on hydraulic investigation. The Hague, The Netherlands.

Nittrouer, C.A., DeMaster, D.J., 1996. The Amazon shelf setting: tropical, energetic, and influenced by a large river. Cont. Shelf Res., 16, 553–573. https://doi.org/10.1016/0278-4343(95)00069-0

Orseau, S., Lesourd, S., Huybrechts, N., Gardel, A., 2017. Hydro-sedimentary processes of a shallow tropical estuary under Amazon influence. The Mahury Estuary, French Guiana. Estuar. Coast. Shelf Sci., 189, 252–266. https://doi.org/10.1016/j.ecss.2017.01.011

Péron, C., Chatelet, A., Gensac, E., Gardel, A., 2013. Mud bank migration from remote sensing and bathymetric data: The example of the Kourou River Estuary, French Guina, South America. J. Coast. Res. Special Issue 65, 558–563. https://doi.org/10.2112/SI65-095.1

Plaziat, J.-C., Augustinus, P.G.E.F., 2004. Evolution of progradation/erosion along the French Guiana mangrove coast: a comparison of mapped shorelines since the 18th century with Holocene data. Mar. Geol., 208, 127–143. https://doi.org/10.1016/j.margeo.2004.04.006

Prost, M.T., 1989. Coastal dynamics and chenier sands in French Guiana. Mar. Geol., 90, 259–267. https://doi.org/10.1016/0025-3227(89)90128-X

Pujos, M., Froidefond, J.-M., 1995. Water masses and suspended matter circulation on the French Guiana continental shelf. Cont. Shelf Res., 15, 1157–1171. https://doi.org/10.1016/0278-4343(94)00062-R

Pujos, M., Latouche, C., Maillet, N., 1996. Late quaternary paleoceanography of the French Guiana continental shelf: Clay-mineral evidence. Oceanol. Acta 19, 477–487. https://doi.org/10.1016/0025-3227(94)90033-7

Rine J. M., Ginsburg R. N., 1985. Depositional facies of a mud shoreface in Suriname, South America: a mud analogue to sandy, shallow-marine deposits. J. Sed. Petrol. 55, 633-652. https://doi.org/10.1306/212F87A6-2B24-11D7-8648000102C1865D

Rodriguez, H.N., Mehta, A.J., 1998. Considerations on wave-induced fluid mud streaming at open coasts. Geol. Soc. Lond. Spec. Publ. 139, 177–186. https://doi.org/10.1144/GSL.SP.1998.139.01.14

Tolman, H. L., 2009: User manual and system documentation of WAVEWATCH III version 3.14. NOAA / NWS / NCEP / MMAB Technical Note **276**, 194 pp.+ Appendices.

Trowbridge, J.H., Kineke, G.C., 1994. Structure and dynamics of fluid muds on the Amazon continental shelf. J. Geophys. Res. Oceans 99, 865–874. https://doi.org/10.1029/93JC02860

van Ledden, M., Vaughn, G., Lansen, J., Wiersma, F., Amsterdam, M., 2009. Extreme wave event along the Guyana coastline in October 2005. Cont. Shelf Res., 29, 352–361. https://doi.org/10.1016/j.csr.2008.03.010

Walcker, R., Anthony, E.J., Cassou, C., Aller, R.C., Gardel, A., Proisy, C., Martinez, J.-M., Fromard, F., 2015. Fluctuations in the extent of mangroves driven by multi-decadal changes in North Atlantic waves. J. Biogeogr. 42, 2209–2219. https://doi.org/10.1111/jbi.12580

Wang, Y., Healy, T., Augustinus, P., Baba, M., Bao, C., Flemming, B., Fortes, M., Han, M., Marone, E., Mehta, A., Ke, X., Kirby, R., Kjerfve, B., Schaefer-Novelli, Y., Wolanski, E., 2002. Chapter One Research issues of muddy coasts, in: Healy, Terry, Wang, Ying, Healy, J.-A. (Eds.), Proceedings in Marine Science, Muddy Coasts of the World. Elsevier, pp. 1–8. https://doi.org/10.1016/S1568-2692(02)80075-4

Wells, J.T., 1983. Dynamics of coastal fluid muds in low-, moderate-, and high-tide-range environments. Can. J. Fish. Aquat. Sci. 40, s130–s142. https://doi.org/10.1139/f83-276

Wells, J.T., Coleman, J.M., 1981a. Physical processes and fine-grained sediment dynamics, coast of Surinam, South America. J. Sediment. Petrol. 51, 1053–1068. https://doi.org/10.1306/212F7E1E-2B24-11D7-8648000102C1865D

Wells, J.T., Coleman, J.M., 1981b. Periodic mudflat progradation, northeastern coast of South America: a hypothesis. J. Sediment. Petrol. 51, 1069–1075. https://doi.org/10.2110/jsr.51.1069

Wells, J.T., Coleman, J.M., 1977. Longshore transport of mud by waves: northeastern coast of South

America. Geol. En Mijnb. 57, 353–359.

Wells, J.T., Coleman, J.M., Wiseman, Wm. J., 1978. Suspension and Transportation of Fluid Mud by Solitary-Like Waves. Coast. Eng. 1978, Proceedings 1932–1952. https://doi.org/10.1061/9780872621909.119

Wells, J.T., Kemp, G.P., 1986. Interaction of Surface Waves and Cohesive Sediments: Field Observations and Geologic Significance, in: Mehta, A.J. (Ed.), Estuarine Cohesive Sediment Dynamics, Lecture Notes on Coastal and Estuarine Studies. Springer New York, pp. 43–65.

Wells, J.T., Prior, D.B., Coleman, J.M., 1980. Flowslides in muds on extremely low angle tidal flats, northeastern South America. Geology 8, 272–275. https://doi.org/10.1130/0091-7613(1980)8<272:FIMOEL>2.0.CO;2

Winterwerp, J.C., Erftemeijer, P.L.A., Suryadiputra, N., Van Eijk, P., Zhang, L., 2013. Defining eco-morphodynamic requirements for rehabilitating eroding mangrove-mud coasts. Wetlands, 33, 515–526. https://doi.org/10.1007/s13157-013-0409-x

Winterwerp, J.C., Graaff, R.F. de, Groeneweg, J., Luijendijk, A.P., 2007. Modelling of wave damping at Guyana mud coast. Coast. Eng. 54, 249–261. https://doi.org/10.1016/j.coastaleng.2006.08.012

Wong, T.E., de Kramer, R., de Boer, P.L., Langereis, C., Sew-A-Tjon, J., 2009. The influence of sea-level changes on tropical coastal lowlands; the Pleistocene Coropina Formation, Suriname. Sediment. Geol. 216, 125–137. https://doi.org/10.1016/j.sedgeo.2009.02.003

List of figure captions

Figure 1. (a) Location map of the study area in northeastern South America, and (b) the French Guiana coast between the Mahury and the Approuague Rivers; (c) the most important commercial harbour (Dégrad-des-Cannes) in French Guiana is located in the mouth of the Mahury and its navigation channel is represented by the thick black line with kilometric intersections. The left side of the estuary mouth is characterized by a rocky outcrop and headland-bound sandy beaches, while the right side is characterized by dense mangroves and a muddy substrate. Offshore bedrock islets are in black. Isobaths were extracted from the 2016 hydrographic survey. Tide gauge and wave buoy stations are represented by black stars and a black circle, respectively. Red lines identify transects where depth values were extracted for Figure 4.

Figure 2. Spatio-temporal diagram of sources of forcing involved in the migration of mud banks.

Figure 3. (a) Location map of transects of yearly hydrographic surveys conducted within and offshore of the Mahury estuary to monitor mud-bank migration; (b) location map of stations where vertical density profiles were collected during phases of low and high wave energy.

Figure 4. Depth sections extracted (a) across-shore and (b) alongshore (see locations in Fig. 1). Cross-shore sections highlight differences in the shape of the mud-bank surface at leading and trailing edges. Longshore sections enable delineation of accretion and erosion areas in shallow waters and identification of the footprint of the subtidal part of the mud bank.

Figure 5. Bed evolutions obtained from digital elevation model (DEM) subtractions of bathymetric survey data in the estuary mouth and the outer mud bank. A sub-layer of the more recent bathymetry ranging between +3 and -15 m (compared to chart datum) is also represented in grey shading. Measurements were realized yearly from 2008 to 2018. DEM subtractions are computed every two years (a-e) and between 2010 and 2018 (f). For the last subtraction, the total difference was computed with the 2010 survey due to the smaller coverage of the 2008 survey which did not include the area off Cayenne (Fig. 1).

Figure 6. Photographs showing the complete filling of the Kourou navigation channel (4.2 m) by a fluid mud patch after a storm event in 2011. The site is located 55 km from the study area and is characterized by a similar configuration with a rocky outcrop stabilizing the left edge of the estuary mouth. The Atlantic Ocean is in the background in photo A.

Figure 7. (a) Spatial distribution of the wet bulk density ($kg.m^{-3}$) obtained from shipboard profiling surveys over the outer mud bank during a high wave-energy phase (February 2014). Bulk density corresponds to averaged values computed in the first 30 cm of the fluid-mud layer. Where the fluid-mud layer is not significant (< 20 cm), the bulk density corresponds to the maximum value measured at the end of the profile; (b) vertical variations of the wet bulk density along a normalized depth at representative stations in leading and trailing edges of the mud bank. Vertical profiles were acquired by a DensiTune probe (Stema Systems) based on the tuning fork method.

Figure 8. (a) Spatial distribution of the wet bulk density ($kg.m^{-3}$) obtained from shipboard profiling surveys over the outer mud bank during a low wave-energy phase (December 2014). Bulk density corresponds to averaged values computed in the first 30 cm of the fluid mud layer. Where the fluid-

mud layer is not significant (< 20 cm), the bulk density corresponds to the maximum value measured at the end of the profile; (b) vertical variations of the bulk density along normalized depths at representative stations in leading and trailing edges of the mud bank. Vertical profiles were acquired by a DensiTune probe (Stema Systems) based on the tuning fork method.

Figure 9. Thickness of fluid-mud layers measured over the outer mud bank during (a) high wave (02/2014) and (b) low wave-energy events (12/2014). Thicknesses were computed from vertical profiles of the wet bulk density acquired with a DensiTune probe. During high wave events, fluid-mud was mainly located in the leading edge and secondarily at the east end of the trailing edge. During calm conditions, fluid mud is only observed in the navigation channel.

Figure 10. (a) Raw and filtered time series of the wave energy criterion (H_0^3/T^2) computed from predicted wave characteristics. Predictions are provided by the WAVEWATCH III global model and extracted at 4.9°N and 307.8°E. Orange points correspond to time averages for periods separating each bathymetric survey (dashed lines). Computed volumes of eroded (light grey) and deposited sediments (dark grey) are represented for each period in (b) the offshore area, and (c) the estuary mouth. Volume computation starts in 2012 and finishes in 2017 due to small coverages of 2008 and 2018 surveys which did not include trailing and leading edges, respectively.

Figure 11. (a) Map of the shoreline and evolution of the 2m-isobath during from 2008 to 2018; (b) 2 m-isobath and (c) shoreline variations since 2008. Isobaths were extracted from bathymetric surveys, and shorelines from Landsat images.

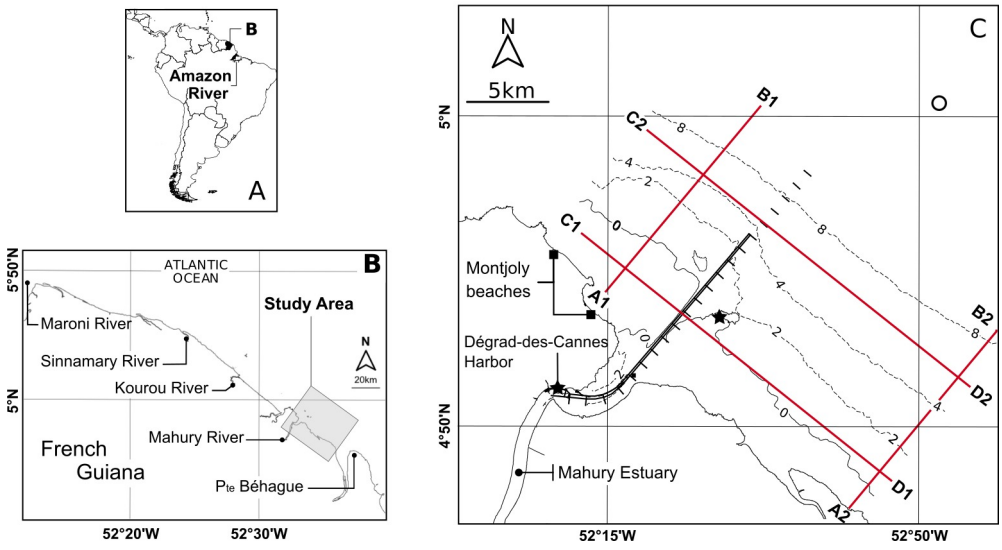
B
Amazon
River
A
ATLANTIC
OCEAN
B
Study Area
Maroni River
Sinnamary River
Kourou River
Mahury River
French
Guiana
Pte Béhague
N
20km
5°50'N
5°N
52°20'W
52°30'W
N
5km
C
5°N
4°50'N
B1
C2
C1
A1
B2
D2
D1
A2
Montjoly
beaches
Dégrad-des-Cannes
Harbor
Mahury Estuary
52°15'W
52°50'W

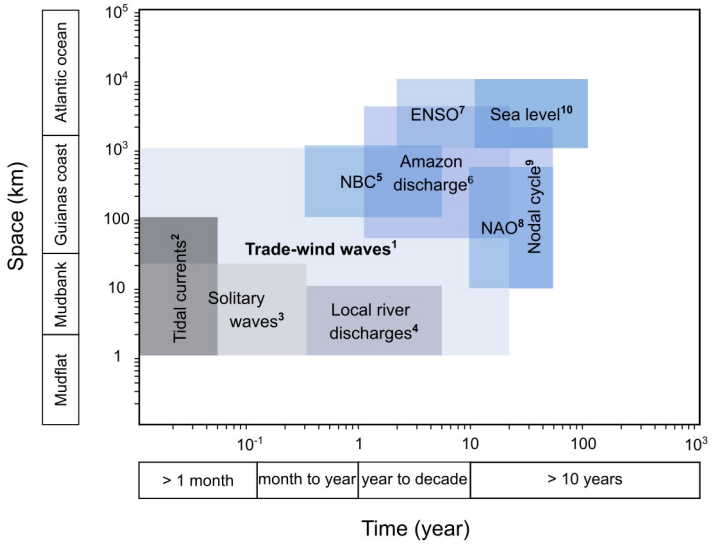

1. Augustinus (1978, 2004), Allison *et al.* (2000), Eisma *et al.* (1991), Gardel and Gratiot (2005), Gratiot *et al.* (2007), NEDECO (1968), Rodriguez and Mehta (1998).
2. Bourret *et al.* (2008), Chevalier *et al.* (2008), Gensac *et al.* (2015), Pujos and Froidefond (1995), Wells and Coleman (1977).
3. Wells *et al.* (1978), Wells and Coleman (1981a).
4. Anthony *et al.* (2013), Anthony *et al.* (2014), Péron *et al.* (2013).
5. Bourret *et al.* (2008), Geyer *et al.* (1996), Pujos and Froidefond (1995).
6. Allison *et al.* (2000), Eisma and van der Marel (1971), Gensac *et al.* (2016), Gibbs *et al.* (1976), Nittrouer and DeMaster (1996).
7. Gratiot *et al.*, (2008), Pujos *et al.* (1996).
8. Walcker *et al.* (2015).
9. Gratiot *et al.* (2008), Wells and Coleman (1981b).
10. NEDECO (1968).

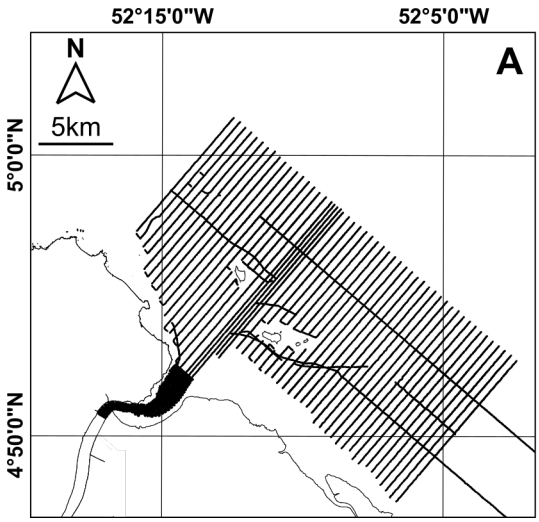
52°15'0"W
52°5'0"W
N
5km
A
5°0'0"N
4°50'0"N

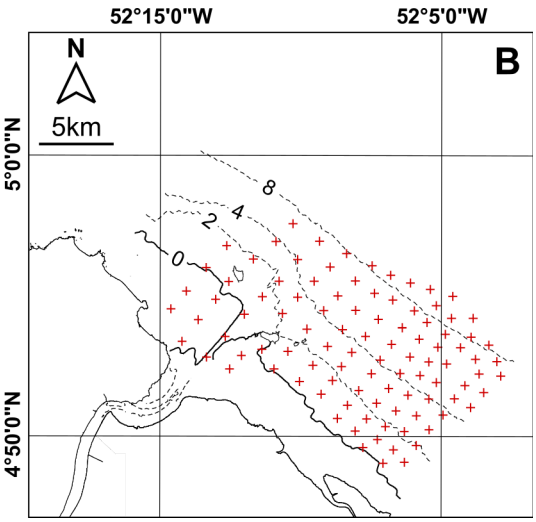
52°15'0"W
52°5'0"W
N
5km
B
5°0'0"N
4°50'0"N
8
4
2
0

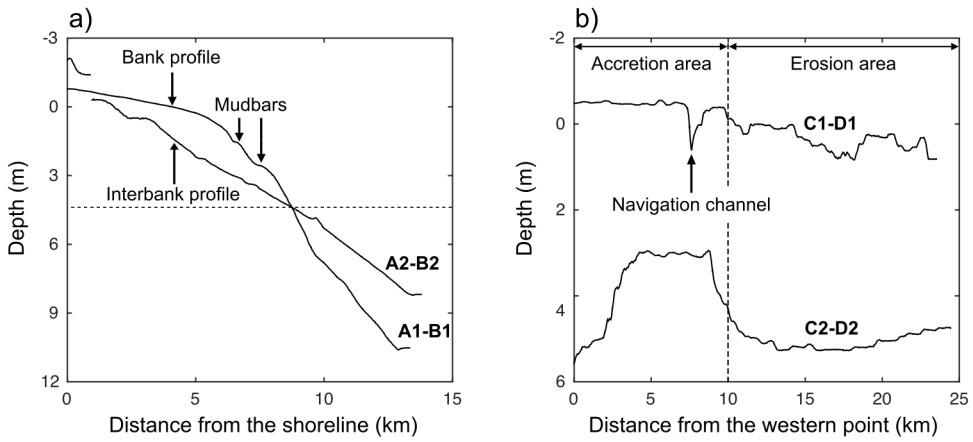
a)
Bank profile
Mudbars
Interbank profile
A2-B2
A1-B1
Depth (m)
Distance from the shoreline (km)
b)
Accretion area
Erosion area
C1-D1
Navigation channel
C2-D2
Depth (m)
Distance from the western point (km)

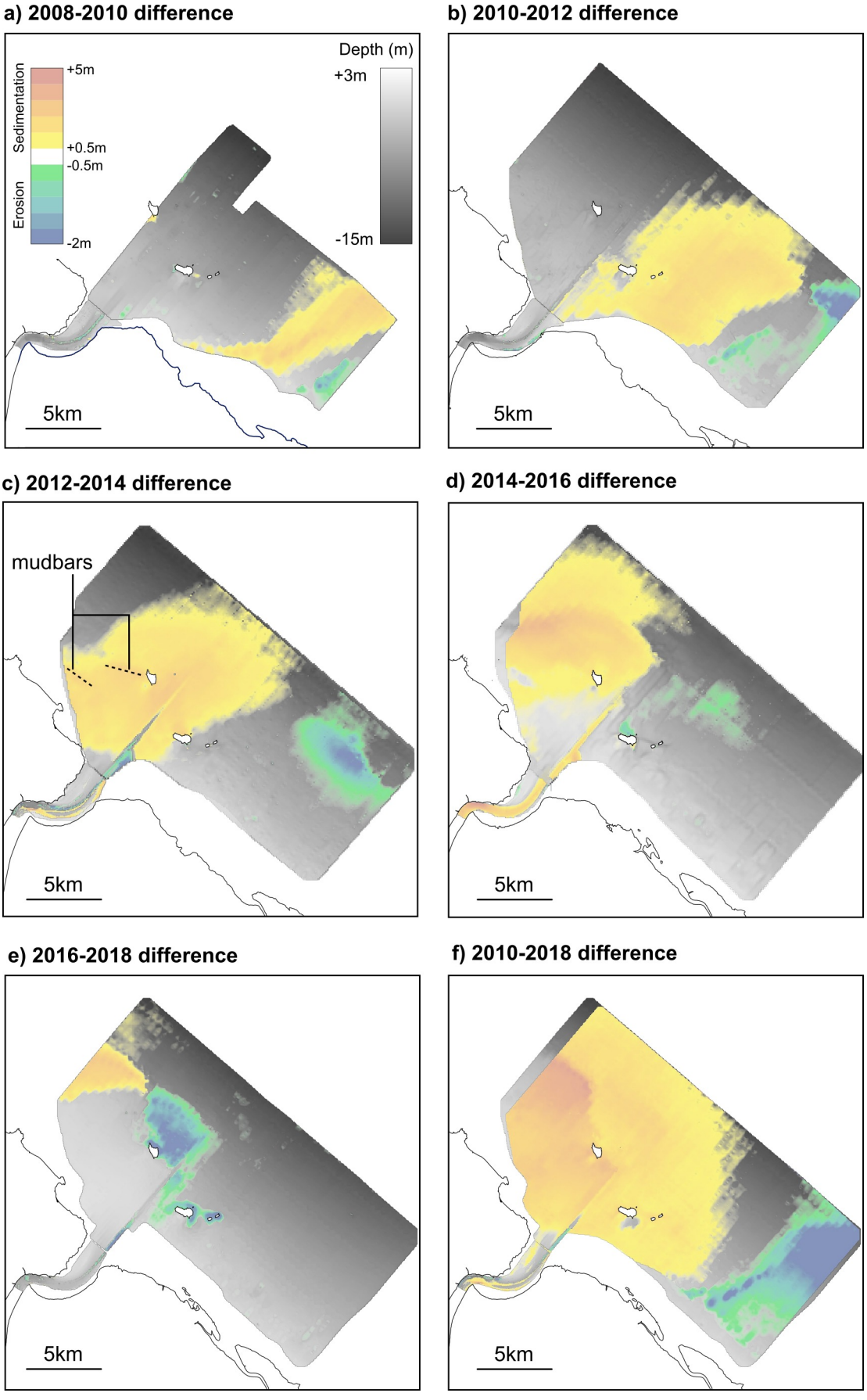
a) 2008-2010 difference
b) 2010-2012 difference
c) 2012-2014 difference
d) 2014-2016 difference
e) 2016-2018 difference
f) 2010-2018 difference
Depth (m)
+3m
-15m
Sedimentation
Erosion
+5m
+0.5m
-0.5m
-2m
mudbars
5km

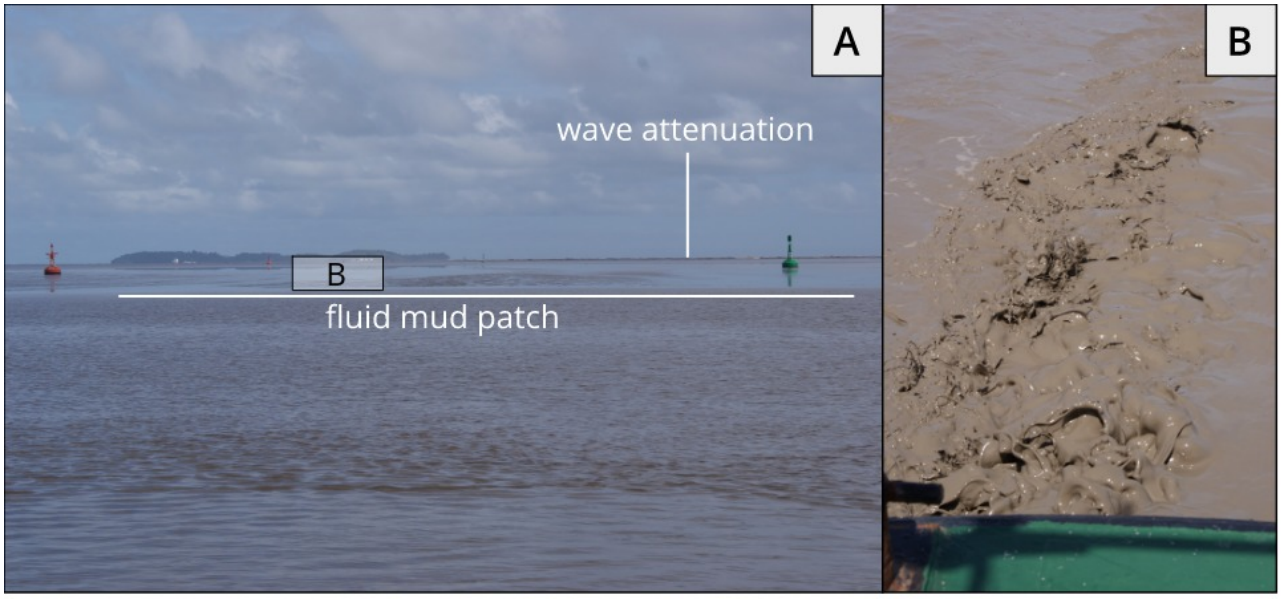
A
wave attenuation
B
fluid mud patch
B

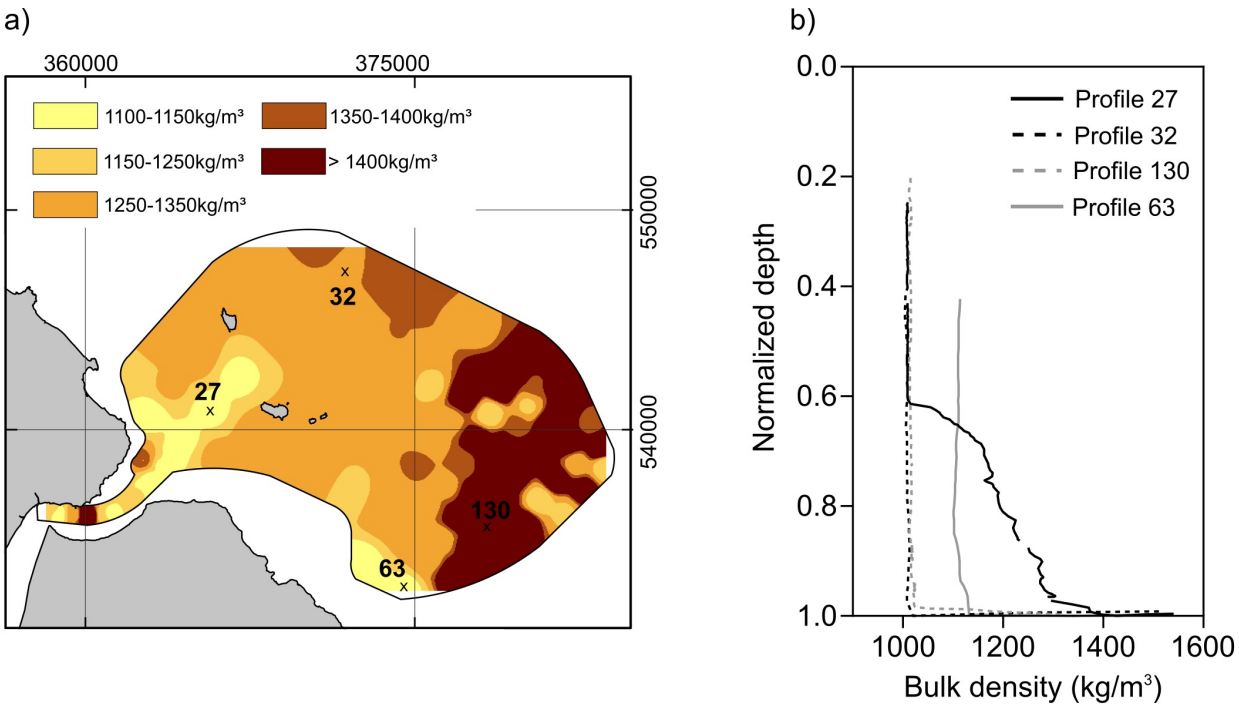
a)
360000
375000
550000
540000
1100-1150kg/m³
1150-1250kg/m³
1250-1350kg/m³
1350-1400kg/m³
> 1400kg/m³
32
27
130
63
b)
0.0
0.2
0.4
0.6
0.8
1.0
Normalized depth
Profile 27
Profile 32
Profile 130
Profile 63
1000
1200
1400
1600
Bulk density (kg/m³)

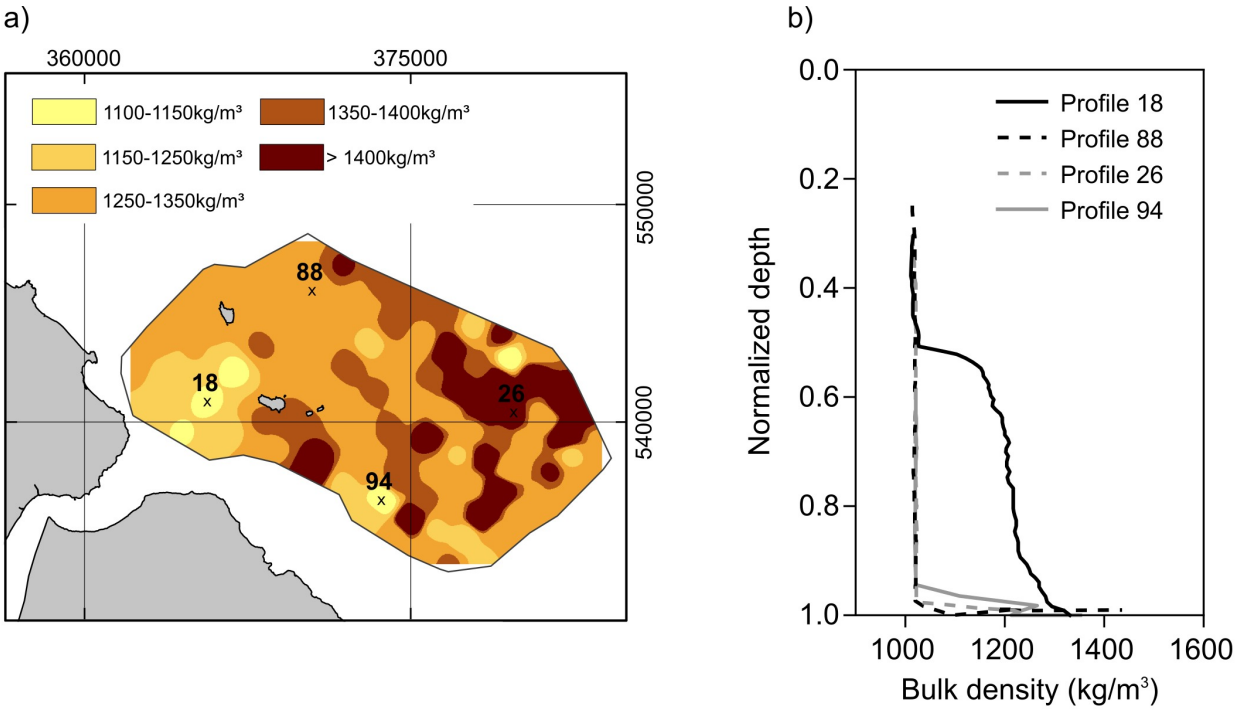
a)
360000
375000
550000
540000
1100-1150kg/m³
1150-1250kg/m³
1250-1350kg/m³
1350-1400kg/m³
> 1400kg/m³
88
18
26
94
b)
Profile 18
Profile 88
Profile 26
Profile 94
Normalized depth
0.0
0.2
0.4
0.6
0.8
1.0
1000
1200
1400
1600
Bulk density (kg/m³)

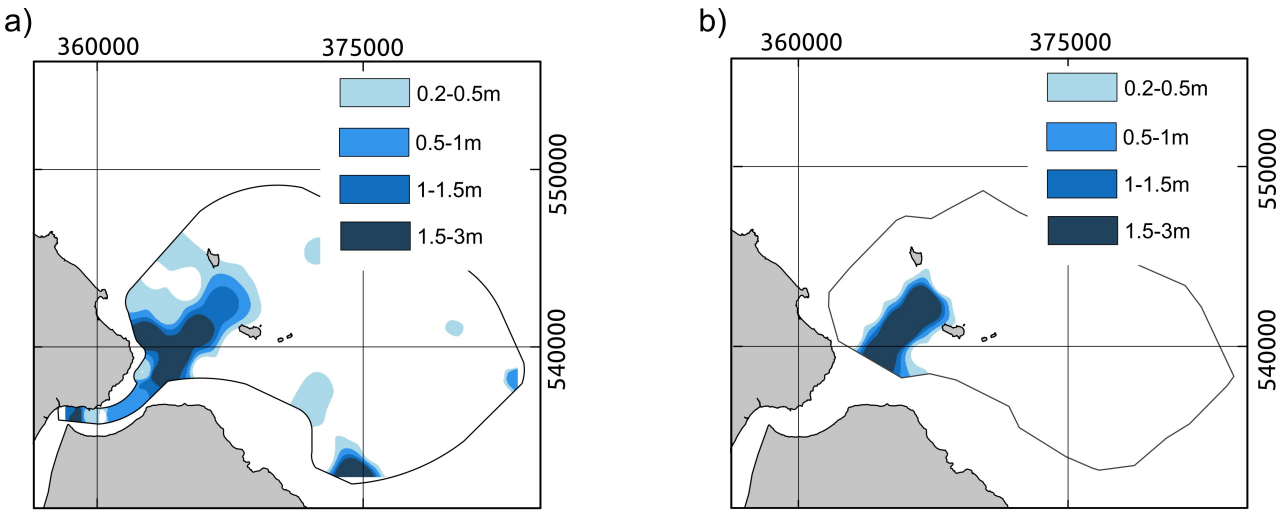
a)
360000
375000
550000
540000
0.2-0.5m
0.5-1m
1-1.5m
1.5-3m
b)
360000
375000
550000
540000
0.2-0.5m
0.5-1m
1-1.5m
1.5-3m

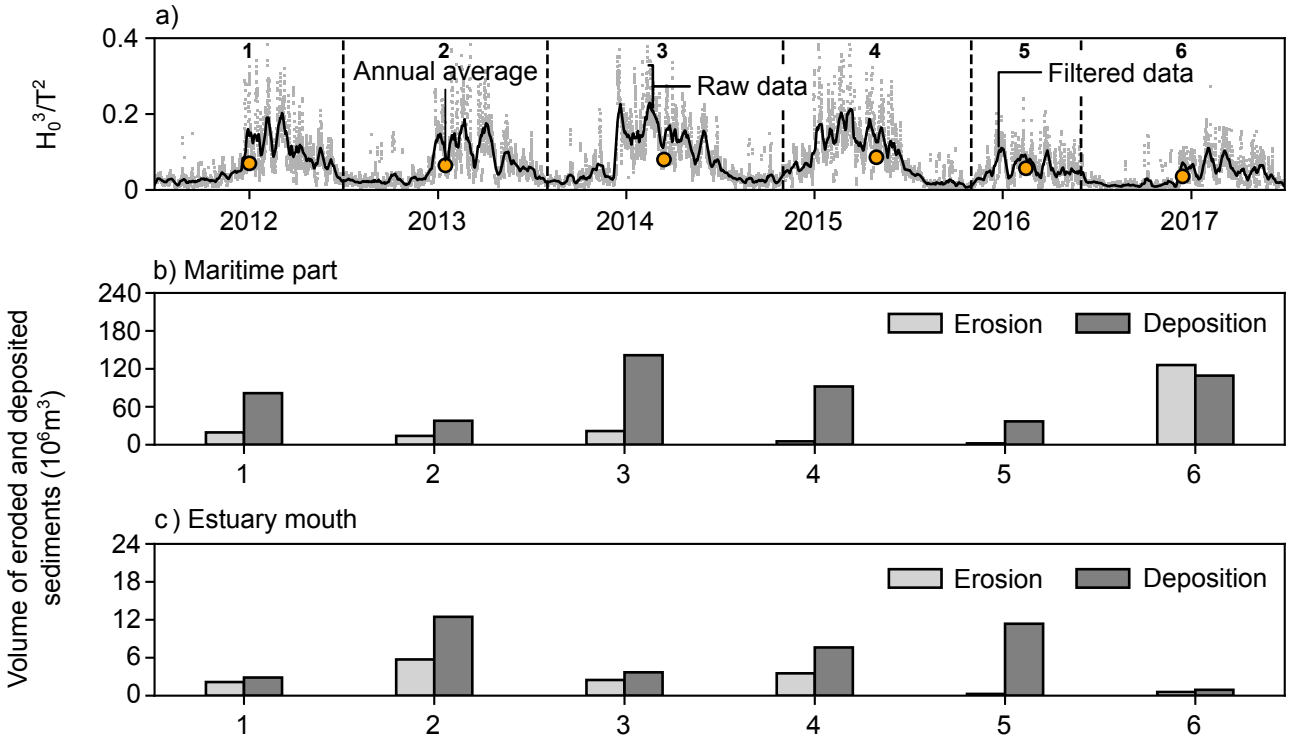
a)
0.4
0.2
0
H_0^3/T^2
1
2
3
4
5
6
Annual average
Raw data
Filtered data
2012
2013
2014
2015
2016
2017
b) Maritime part
240
180
120
60
0
Erosion
Deposition
1
2
3
4
5
6
c) Estuary mouth
24
18
12
6
0
Erosion
Deposition
1
2
3
4
5
6
Volume of eroded and deposited sediments ($10^6 m^3$)

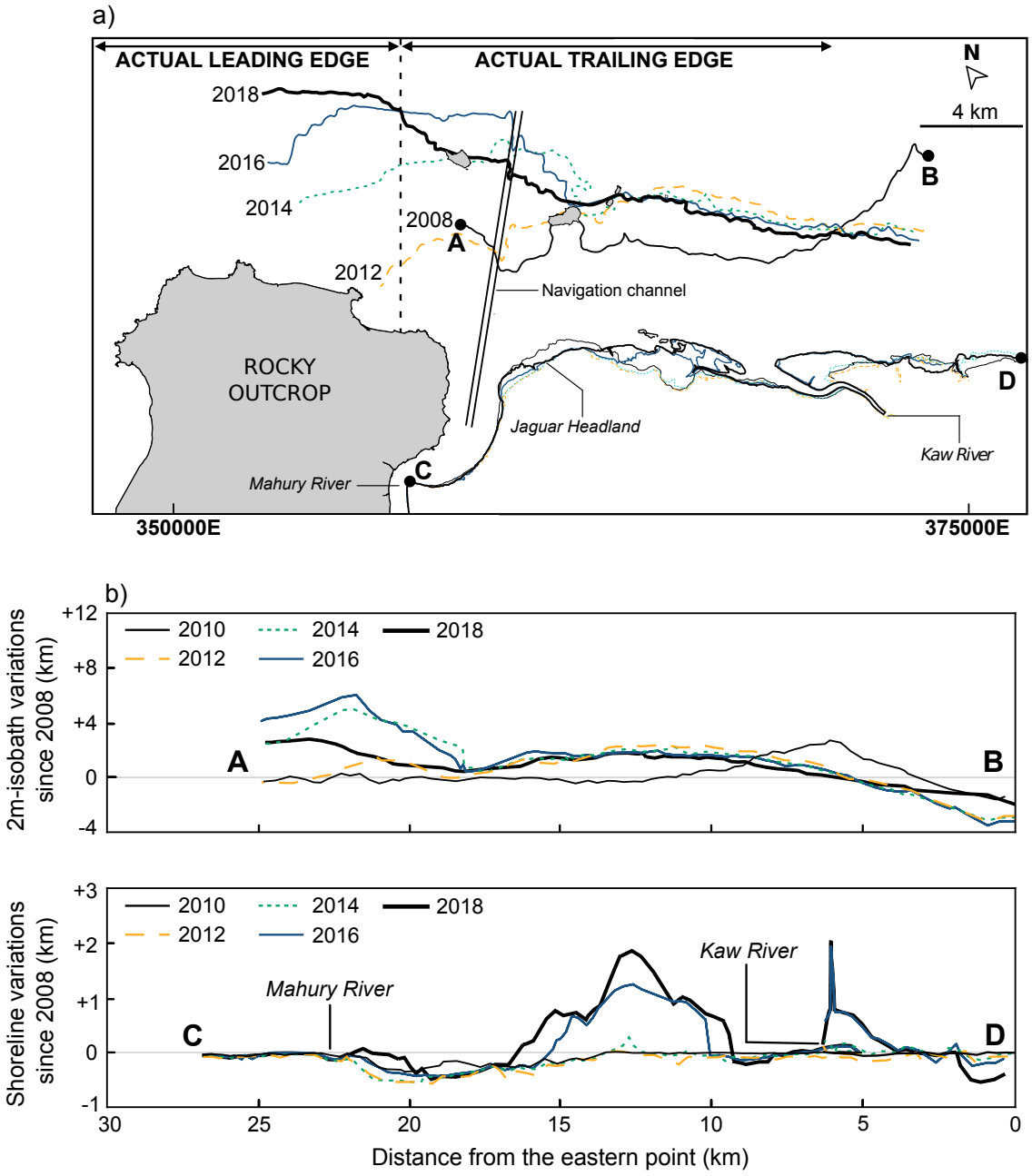
a)
ACTUAL LEADING EDGE
ACTUAL TRAILING EDGE
N
4 km
2018
2016
2014
2012
2008
A
B
C
D
Navigation channel
ROCKY
OUTCROP
Jaguar Headland
Kaw River
Mahury River
350000E
375000E
b)
2m-isobath variations since 2008 (km)
+12
+8
+4
0
-4
2010
2012
2014
2016
2018
A
B
Shoreline variations since 2008 (km)
+3
+2
+1
0
-1
Mahury River
Kaw River
C
D
30
25
20
15
10
5
0
Distance from the eastern point (km)